Current status of self-organized epitaxial graphene ribbons on the C face of 6HSiC substrates

Nicolas Camara, Antoine Tiberj, Benoit Jouault, Alessandra Caboni, Bilal Jabakhanji, Narcis Mestres, Philippe Godignon, Jean Camassel

Current status of self-organized epitaxial graphene ribbons on the C-face of 6H-SiC substrates

Nicolas Camara [1], Antoine Tiberj [2], Benoit Jouault [2], Alessandra Caboni [1], Bilal Jabakhanji [2], Narcis Mestres [3], Philippe Godignon [1] and Jean Camassel [2]

[1] IMB-CNM-CSIC, Campus UAB 08193-Bellaterra, Barcelona, Spain

[2] GES, UMR-CNRS 5650, Université Montpellier 2, 34095-Montpellier cedex 5, France

[3] ICMAB-CSIC, Campus UAB 08193- Bellaterra, Barcelona, Spain

Abstract

The current status of long, self-organized, epitaxial graphene ribbons grown on the (000-1) face of 6H-SiC substrates is reviewed. First, starting from the early stage of growth it is shown that on the C-face of 6H-SiC substrates the sublimation process is not homogeneous. Most of the time it starts from defective sites, dislocations or point defects, that define nearly circular flakes surrounded by bare SiC. These flakes have a volcano-like shape with a graphite chimney at center, where the original defect was located. At higher temperature a complete conversion occurs, which is not yet homogeneous on the whole sample. This growth process can be modified by covering the sample with a graphite cap. It changes the physics of the surface reconstruction during the Si-sublimation process and, on the C-face, makes more efficient the reconstruction of few selected terraces with respect to the others. The net result is the formation of strongly step bunched areas with, in between, long and large reconstructed terraces covered by graphitic material. Despite the low intrinsic optical absorption of few graphene layers on SiC, micro-transmission experiments, complemented by micro-Raman spectroscopy, demonstrate that most of this graphitic coverage is made of one or two homogeneous graphene layers. We show also that most of the thermal stress between the graphene layer and the 6H-SiC substrate is relaxed by pleats or wrinkles which are clearly visible on the AFM images. Finally, the results of transport experiments performed on the graphitic ribbons reveal the p-type character of the ribbons.

1. Introduction

Graphene has emerged recently as a new material with outstanding electronic properties [1-3]. This includes unusual Quantum Hall effect and ballistic transport properties up to room temperature and good compatibility with silicon planar technology. Graphene-based devices are then promising candidates to complement silicon in the near generation of high frequency electronic devices [4]. Such a development of graphene-based technologies necessitates large diameter wafers with uniform graphene coverage. To this end, different growth techniques have been developed to fabricate mono or bi-layer graphene. They range from exfoliated graphite, either mechanically [1, 3] or chemically in a liquid-phase solution [5], to chemical vapor deposition on a metal surface [6, 7] or, more recently, to substrate-free synthesis when passing ethanol into an argon plasma [8]. An alternative method is the one investigated in this work. It consists in a controlled sublimation of few atomic layers of Si from a single crystalline SiC surface [2, 9].

Sublimation is a well-known process in solid state physics which consists in a direct transformation from a solid in a gas phase. For binary compounds, like SiC, stoichiometry is not conserved. The less tightly bound atoms in the solid sublimate first, leaving behind few layers of nearly free C species. Then the C species rearrange (reconstruct) on the underlying SiC substrate to minimize energy. In graphene technology, this reconstruction process in which the SiC substrate plays a major role is known as "epitaxial growth" (EG). Such epitaxial growth of graphene seems to be the most suitable option for industrial applications [4, 6, 10-12]. Four inches semi-insulating SiC wafers are already available and, on top of them, one needs to grow either a large and continuous sheet of monolayer graphene (MLG) or few layers of graphene (FLG) covering homogeneously the full wafer surface. In both cases, controlling the early stage of growth is a prerequisite to get uniform and homogeneous coverage.

At low pressure conditions, i.e. for pressure varying from ultra high vacuum (UHV below 10^{-9} Torr) to standard secondary vacuum (SSV in the range of 10^{-8} to 10^{-6} Torr) it remains challenging to grow FLG on the Si-face of hexagonal SiC substrates with homogeneous domain size larger than few hundred nanometers [13-15]. Low pressure sublimation from the C-face leads to wider domains (and higher

mobility) than the sublimation from the Si-face [11] but, still, it remains difficult to process homogeneously a full SiC wafer. To increase homogeneity, one has to lower the sublimation rate. On the Si-face, this was done independently by Virojanadara *et al* [16] and Emtsev *et al* [17]. Both groups demonstrated that, performing graphitization on the Si-face of a 6H-SiC substrate under Ar close to atmospheric pressure, one could get large, homogeneous, graphene monolayers and bilayers on the $6\sqrt{3}\times 6\sqrt{3}$ reconstructed parts of the SiC surface. Unfortunately, on this Si face, an intermediate C-rich layer made of carbon with sp^2 and sp^3 hybridizations is also created between the SiC substrate and the first layer of graphene. The effect of this so-called "buffer layer" on the electronic transport properties in the graphene layer is clear. It gives donor states which results in a sheet carrier density of the order of 10^{13} cm^{-2} with room temperature mobility (μ_{RT}) below 1000 $cm^2V.^{-1}s^{-1}$. To some extent, this can be cured using hydrogen passivation [18] but the effect is reversible and the long term stability of devices obtained in this way remains to be demonstrated. On the other hand, when graphitizing on the C-face there is no need for a buffer layer. It was then reported that mobility values as high as 27.000 $cm^2\,V^{-1}\,s^{-1}$ could be achieved in FLG grown in this way, but with a rather large number of graphene layers [9].

The primary objective of this work is to review in some detail the main steps that lead to the growth of large, isolated, monolayer graphene ribbons on the C-face of a 6H-SiC substrate. To this end we present, first, the results of standard growth techniques under secondary vacuum. Then we demonstrate that an alternative way exists, which consists in placing a graphitic cap on top of the C-face surface during sublimation. This alternative technique opens a route to grow large, homogeneous, self-organized and (almost) free-standing graphene ribbons on the C-face of a SiC substrate. Investigation of their optical properties will be implemented and, from the results, it will be shown that they are true monolayer and bi-layer graphene. Finally, electrical devices will be done and the electrical properties of the graphene ribbons will be investigated.

2. Experimental details

Surface preparation work. All SiC substrates were 1x1 cm^2 templates cut from a 3-inch, on-axis, semi-insulating 6H-SiC wafer from Cree. Before cutting, electrochemical polishing was done by Novasic to get Epiready® morphology [19]. Then a sacrificial oxide was thermally grown and chemically etched in HF to remove any (small) trace of sub-surface damage that could remain from the polishing process. Next, after cutting and before loading, standard RCA chemical treatments were done to remove any trace of surface contamination. All the treatment was clean-room compatible and similar to the one used for SiC before thermal oxidation or post-implantation annealing. An AFM picture of the atomically flat surfaces obtained in this way is shown in figure 1. The step height is about one Si-C bilayer. The terrace width is ~ 200 nm. Only seen are (weak) residual polishing traces.

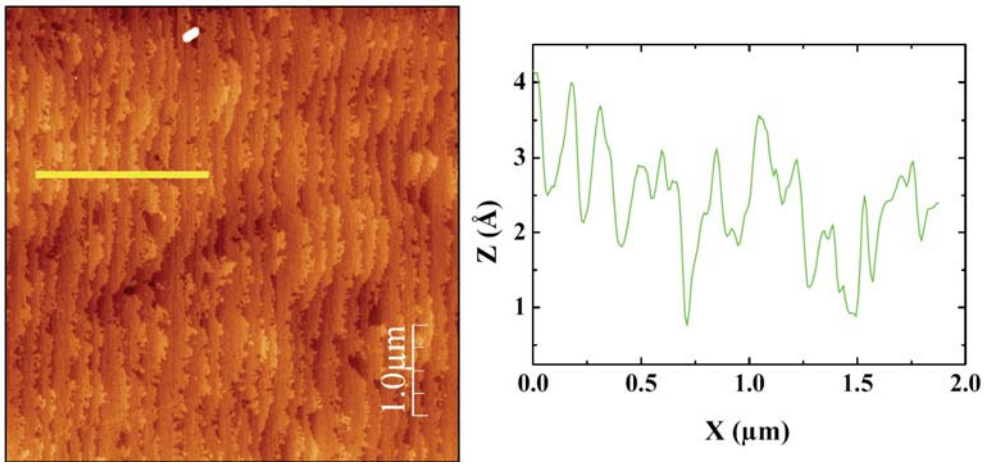

Figure 1. AFM image of a SiC surface (C-face) before loading for graphitization and its corresponding profile.

Graphene growth. For sublimation, we used a high temperature furnace from Jipelec [20], previously dedicated to post-implantation annealing. It was RF-induction heated and fitted with a turbo-molecular pump. The lowest pressure available was ~ 10^{-6} Torr, typical of SSV conditions. Using the same surface preparation technique, several tens of samples were graphitized. Every time, after loading the sample the thermal ramp stopped when the temperature reached 1100°C. Then the sample was heated for 10 minutes to remove any trace of native oxide. For the remaining part the pressure remained set to 10^{-6} Torr and only three parameters were varied : first, the time of growth (from 5 to 60 min) ; second, the

growth temperature (from 1450°C to 1750°C) and, finally, the sample protection state (being covered by a graphite cap or not). We have found the following. Without any protection, the growth is extremely fast and very difficult to control. However, still, there are some physical bases that can be detected. First, a minimal temperature is needed to start the surface transformation process. Using our experimental set-up, this temperature is about 1450ºC but this is not yet a graphitization temperature. It marks simply the onset of surface reconstruction. Instead of monolayer steps, the samples start exhibiting large step-bunched terraces, without any trace of graphene growth. Increasing further the temperature (typically by 50°C) for the same time duration (5 min) an early stage of growth (ESG) is reached. The wafer coverage is not yet complete and, to reach the full graphene coverage (FGC) state one needs to increase the temperature again (to 1550ºC for 5 minutes), unfortunately degrading the step bunched aspect of the SiC surface. Detailed analyses will be given in the next sections, but the most important point is that using a graphitic cap to cover the sample one can increase the partial pressure on the sample surface. In this way, graphitization can be done at higher temperature (from 1700ºC to 1800ºC) and for a longer time (from 15 min to 60 min) without loosing control of the SiC surface step bunching rearrangement. It is still impossible to reach true FGC but, instead, long and homogeneous monolayer and/or bilayer graphene ribbons can be found, all aligned in the same direction on top of large reconstructed terraces.

3. Early stage of growth

Let us first consider the case of samples treated at 1450°C for 5 minutes. The only noticeable effect is a large reconstruction of the initial terraces. This is shown in figure 2. Such extended surface reconstruction is well known in the SiC literature and originates from the small (non intentional) miscut of the (nominally) on-axis 6H-SiC wafer. In most cases, it does not correspond to a single Si-C bilayer (BL) height (0.25 nm) but rather to the height of a half unit cell of the investigated polytype (0.75 nm in 6H and 0.5 nm in 4H, respectively). Most probably, this comes because the surface energy is lower at half of the unit cell, where is positioned the hexagonal turn in 6H and 4H-SiC. When many steps come close together, the result is known as “step bunching” and, in the case of figure 2, this results in large

parallel terraces with ~ 1 nm high and 1-2 µm width. As already said, at this stage under SSV conditions no evidence of graphene formation can be found after 5 min processing. This is true on, both, 6H-SiC [21] and 4H-SiC [22]. For instance, despite intensive research no evidence of graphene formation could be found using Raman spectroscopy in the back-scattering configuration in the work of Ref.[21]. No evidence of Si aggregation before out-diffusion was also found. All together this shows that working at sub-threshold temperature under SSV, no sublimation of Si atoms does occur. Simply the surface reorganizes in order to minimize energy.

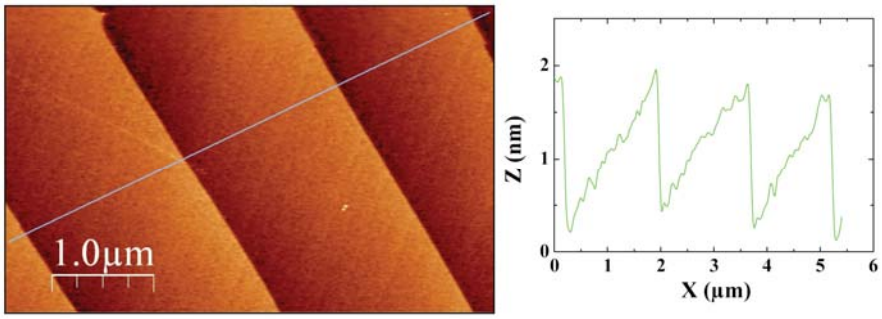

Figure. 2. AFM image and corresponding profile of the step bunching experienced by a 6H-SiC wafer after heating at 1450°C for 5 minutes. No graphene formation could be observed when annealed at such sub-threshold conditions.

Considering now the ESG sample treated at 1500°C for 5 minutes, the situation is entirely different. Many isolated graphene flakes appear which are randomly distributed, with nearly circular shape and almost identical diameter. This is shown in figure 3. In this specific case all graphene flake diameters are in the range of few microns with, still, in between bare step-bunched SiC terraces. These flakes can be seen using AFM (figures 3(a) and 3(b)) or SEM (figures 3(c) to 3(f)) or, even, OM (figures 3(g) and 3(h)). Their density is about 10^6 cm^{-2} over a full sample, which is the typical density of dislocations in a commercial (research grade) SiC wafer. This suggests that threading dislocations act as catalyzing defects, of which the sublimated Si species can more easily escape. Recently, it was also suggested that dislocations may not be the only source of graphene flakes formation and that point defects should play a role [22]. Whatever is the origin, the in-plane shape of the flakes is rather circular. Considering that the growth starts from an extended defect, which acts like a chimney for a volcano, this is not so surprising. All constituting Si atoms in the topmost Si-C BLs must be progressively pumped out by the

central chimney, until some frontier is reached probably corresponding to the diffusion length. No evidence of graphitic materials is found outside the flakes, neither by AFM (figures 3(a,b)), nor by SEM (figure 3(c-f)), nor by OM (figures 3(g,h)).

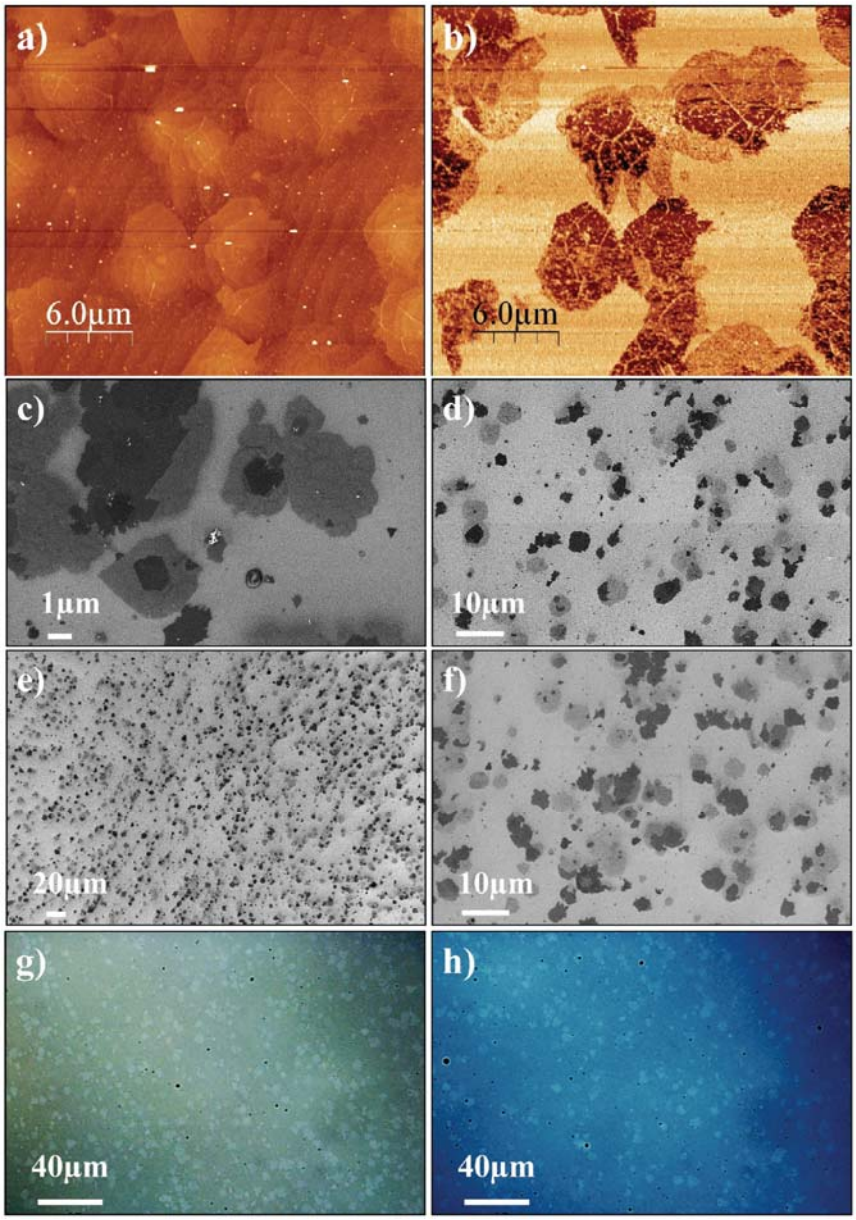

Figure 3. Summary of results collected on an ESG samples after heating at 1500°C for 5 min. AFM images in (a) topography and (b) phase mode. (c-f) SEM pictures of the early growth flakes: the darker flakes visible at SEM correspond to a higher number of graphene layers. (g,h) Wide range optical microscope viewgraphs with many different flakes clearly visible: the brighter the thicker.

This was easily confirmed using Raman spectroscopy. Well-resolved graphite G-band and 2D-band were found inside the flakes, giving absolute evidence of carbon sp^2 re-organization [23-25] but not homogeneously within the same flake or from flake to flake. This is not so surprising when considering

the AFM phase mode picture in figure 3(b): inside every flake we find always a combination of different colors indicating several (different) graphene thicknesses. Altogether, these results suggest that there is a large energy barrier which forbids the (direct) diffusion of Si atoms through the topmost carbon layer or that nucleation center originating from surface defects is much more efficient.

This was confirmed by the results of an ab initio calculation performed in the work of Ref.[21]. To evaluate the energy needed for a Si atom (located 1.99 Å below the first graphene layer) to move outside, two different geometries were assumed: i°) a perfect (infinite) honeycomb lattice and ii°) a defective topmost layer with a so-called Stone-Wales defect [26]. In the defect-free carbon layer, the lateral (x,y) positions of the Si atom corresponded to the center of an unperturbed hexagon. With the Stone-Wales defect, it was fixed at the center of one defective heptagons as seen in figure 4.

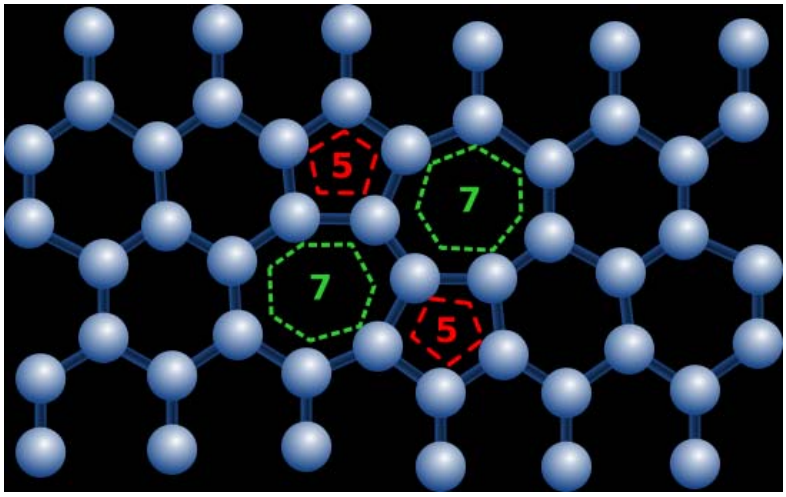

Figure 4. Schematics of a Stone-Wales defect. Different configurations may exist, but always combine one heptagonal and one pentagonal feature. For details, see Ref.26

The diffusion barriers calculated in this way ranged from 15.6 eV for the direct jump through a perfect layer to 9.7 eV in the presence of a Stone-Wales defect. This is very large and has two consequences. First, it makes very difficult the direct jump of an in-depth Si atom to the topmost graphene layer in order to sublimate. Second, with a structural defect the jump becomes easier but, still, is hardly possible. In other words, going through a small localized defect lowers the sublimation energy but this is not enough to account for the strong difference noticed between the results of figure 2 and the

ones of figure 3 for only 50°C difference. The fast sublimation of Si atoms noticed in figure 3 requires a much larger defect, like a threading dislocation for instance.

4. Full wafer coverage

Consider now the sample FGC graphitized at 1550°C for 5 min under SSV. The situation is entirely different. Compared to the previous sample grown at only 50°C lower temperature, the whole surface is now covered with graphene, with no trace of bare SiC anymore. This appears clearly in figure 5 from the OM, SEM and AFM pictures. Unfortunately; they show also that this full graphene coverage (FGC) is not homogeneous in terms of graphene thickness but, instead, varies very rapidly at the micrometer scale.

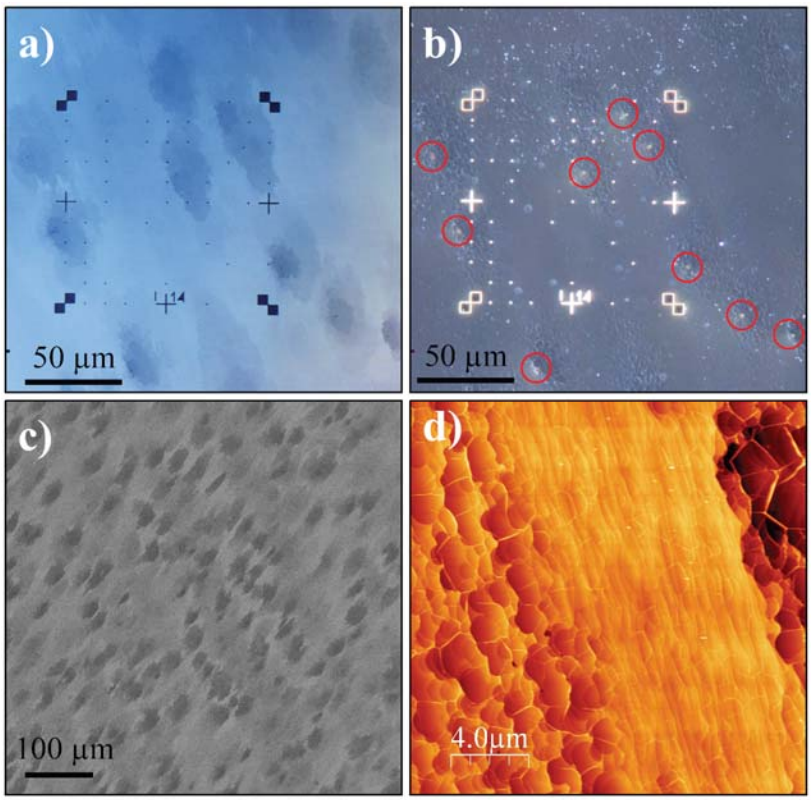

Figure 5: Wide range OM view of the samples FGC graphitized at 1550°C during 5 min (a) in cross-polarized mode and (b) in dark field mode with superimposed red circles highlighting the apparent treading dislocation present in the SiC substrate and originating the thicker (darker and rougher) graphene flakes. (c) Wide range SEM view of the same kind of samples. In between the thicker flakes, a light continuum is visible by OM and SEM when the flakes coalesce and can be distinguished by (d) AFM measurements. The thicker areas are rougher with terraces much more disturbed.

In figure 5(a) and figure 5(c) the dark parts seen by cross-polarized mode OM and by SEM are main chimneys, already identified in the previous section. In between there is a light continuum with less graphene layers. This suggests that the thermal energy provided to the SiC system at such growth conditions is sufficient to insure the coalescence of all circular flakes found in the previous sample, but cannot insure homogeneity. Moreover, from the dark field mode shown in figure 5(b) and the AFM picture in the topography mode in figure 5(d), it appears clearly that the thicker the graphene flakes, the more the surface is disturbed and rough with the initial step bunching disappearing. In between, in the light continuum, the surface is much less destroyed and some steps order is still conserved.

To summarize, the standard SSV conditions allows the formation of FLG flakes covering the whole SiC sample but, unfortunately, they are not at all homogeneous [11, 21]. This comes because the starting sublimation process is not intrinsic. Defects like threading dislocations [21] (rather than point defects [22]) localize the escape process living behind a strongly inhomogeneous surface reconstruction pattern. Using OM (Optical Microscopy) in both the cross-polarization mode and the dark field mode one evidences easily the growth features associated with the two main processes. The cross-polarized mode allows seeing very clearly the darker areas corresponding to a large number of graphene flakes while in the dark field mode, as seen highlighted by red circles in figure 5(b), some crystallographic defects reveal. They appear as yellow cones of diffracted light in the center of thick flakes, from which seems to originate the growth. Defocusing the microscope a few microns down to the surface in the dark field mode, these threading dislocations appear even more clearly and, in the case of transparent on-axis wafers, produce long yellow beams. In this case, merging the pictures of both modes, we can see very easily in figure 6 that almost every thick flake has nucleated from a dislocation already present in the starting SiC wafer.

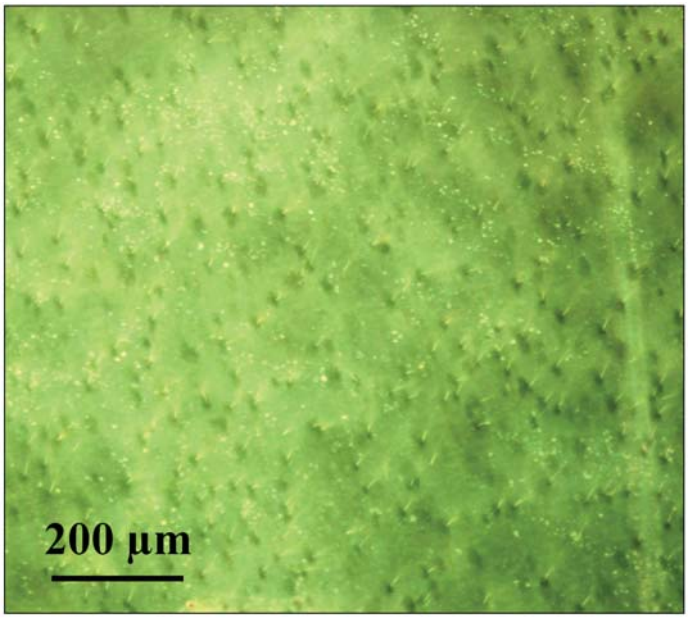

Figure 6. Merged picture of wide range optical microscopy in the cross-polarized mode and in the dark-field mode. The sample is fully covered by FLG grown at 1550°C under SSV. The thicker FLG areas appear darker and originate from threading dislocations visible as yellow beams in the dark field mode.

To estimate more in detail the quality and uniformity of our graphitic material; we performed Raman spectroscopy measurement on different samples in many different areas. We have found the following :

- Probing with the Raman laser beam the different areas seen by SEM in figure 7(a), we find that the G-band and 2D-band intensities shown in figure 7(b) vary by (at least) a factor 10 to 20 when moving from the light continuum (green spot in figure 7(a) and bottom spectrum in figure 7(b)) to the center of a thick dark area (red spot and upper spectrum in figure 7(b)). Since these G and 2D band intensities directly connect to the graphene thickness, this confirms, on a pure experimental basis, that we are really dealing with strongly different thicknesses.

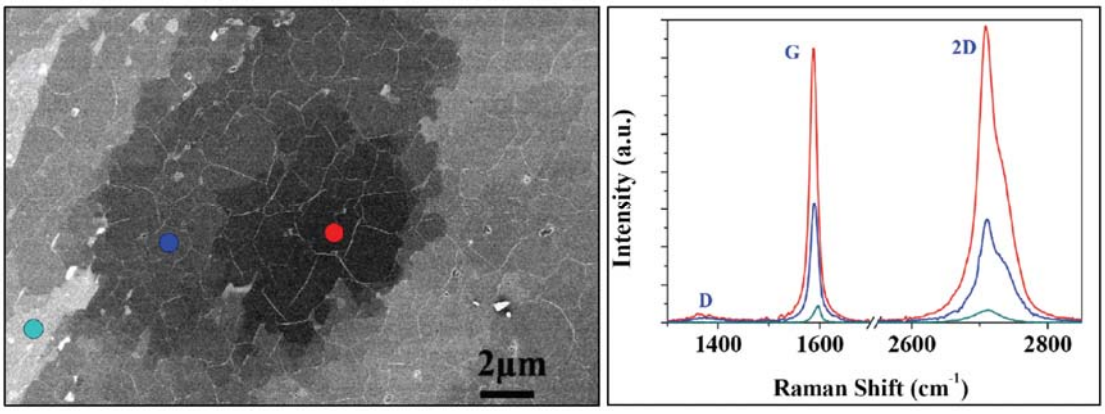

Figure 7. (a) SEM picture of a thick graphitic flake grown on the C-face of a SiC substrate under standard SSV condition at 1550ºC during 5 minutes; (b) Raman spectra collected on the same sample in three different parts corresponding to the different colored spots in the SEM picture. From bottom to top spectra the number of graphene layers increases by, typically, a factor of 10 and the shape of the 2D-band evolves differently from EG grown on the Si-face of a SiC substrate (see text).

- In the case of EG grown on the Si-face of a SiC substrate, it is well known that the staking of the graphene layer is mostly Bernal (AB stacking) [27], and the shape of the 2D band being extremely stacking-order sensitive [23, 28], it is then relatively easy to extract from the Raman signal the number of graphene layers. When grown on the C-face of a SiC substrate, the stacking order of the graphene layers is much less trivial to know. This is due the fact that there is almost ***no*** coupling between the first layer and the substrate and, as a consequence, the graphene layers are almost randomly oriented. Consider for instance the green spot (uniform continuum in figure 7(a)) most of the spectra exhibit a 2D-band at 2710 cm^{-1} with a full width at half maximum (FHWM) of about 42 cm^{-1}. This corresponds to standard turbostratic graphite which, in our case, is made of rather few graphene layers.
- On the opposite, focusing on the thicker graphene parts (blue and red spots in figure 7(a)) we find a clear broadening and multi-peak structure of the 2D-band coming from the splitting of the band structure at Dirac K points. This reveals better with the intermediate thickness (blue spot) than the very thick one (red spot) most probably due to different couplings between the Bernal parts in the staking sequence.
- For the shake of completeness, let us finally discuss the case of very thick EG (of the order of several tens of nanometer thickness) grown at higher temperature (in the range of 1600ºC for 10 to 20minutes). In this case, we have observed Raman signatures in which the SiC signal is ***not*** visible anymore but amazingly, using such growth conditions, the Raman spectrum may be very close to the one of a single graphene layer. This is shown in figure 8. The 2D-band intensity is extremely large (much higher than the one of the G band) with FWHM of about 23 cm^{-1} and Raman shift at about 2696 cm^{-1}. This is a confirmation, by the Raman spectroscopy method, that the material grown at high temperature on the C-face of a SiC substrate is thick graphite made of tens of randomly

rotated graphene layers [27, 29]. Nevertheless, the D-band at 1380 cm^{-1} and the small shoulder on the right hand side of the G-band are signs of defects and/or rather small domains. Also the right hand side shoulder of the 2D-band reveal that the staking is not completely disordered but that, probably, some coupling between layers still occurs.

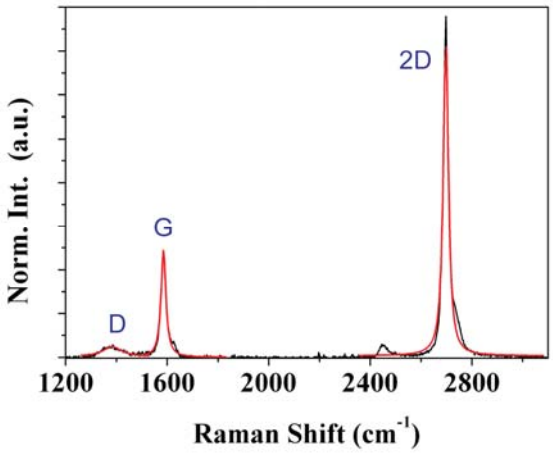

Figure 8. Example of Raman spectra collected for very thick EG on the C-face SiC substrates. In such a case the SiC Raman signal is almost invisible and the spectrum is very similar to the one of a single graphene monolayer.

To conclude, considering the "standard" epitaxial growth of graphene on the C-face of a SiC substrate, our last comment is that, after hundreds of Raman tests, we have never been able to detect any signal from a single graphene layer (even in the thinnest zone). We are confident that, using such standard parameters as SSV and growth temperature in the range of 1500 to 1600°C, it will be extremely difficult to reach what many groups are looking for: a large monolayer of graphene covering the whole sample surface. Considering that the growth process under SSV was not expected to produce a large and homogeneous pavement of uniform graphene sheets covering a full SiC wafer, a new specific and radically different growth technique was developed.

5. Use of a graphite cap

Up to now we have shown that, working under SSV conditions, the graphitization of 6H-SiC is not an intrinsic process. The basic reason is that any existing structural defect creates a nucleating center which is much more efficient than the spontaneous growth process which requires more energy to occur. As a consequence, to grow large and homogeneous graphene layers, this extrinsic process has to be

controlled. The main idea was to focus on this defect-assisted growth and optimize it. To this end, a key is to cover the SiC sample with a graphite cap [30]. Increasing the C and Si partial pressure at the surface of the SiC sample, one lowers the Si sublimation rate while still keeping a rather large diffusion length for the Si and C species. At 1550°C this results in a complete quenching of the graphite growth. There is ***no*** graphene layer anymore but, simply, a large reconstruction of the wafer surface.

To see EG layers again, one needs to raise the temperature to ~ 1700°C for about 15 minutes. There is still no full wafer coverage but, instead, a large number of long, self-organized, graphene ribbons which appear clearly in figure 9(a) (OM picture in the dark field mode) and/or figure 9(b) (SEM). In both cases, it is obvious that using such new growth conditions the graphene flakes already nucleated around surface defects still exist but they are much longer, more homogeneous, far from coalescence and running massively parallel. Last but not least, in between are not thin EG layers but simply nude SiC areas which renders easier the processing technology (see Section 10 for more details).

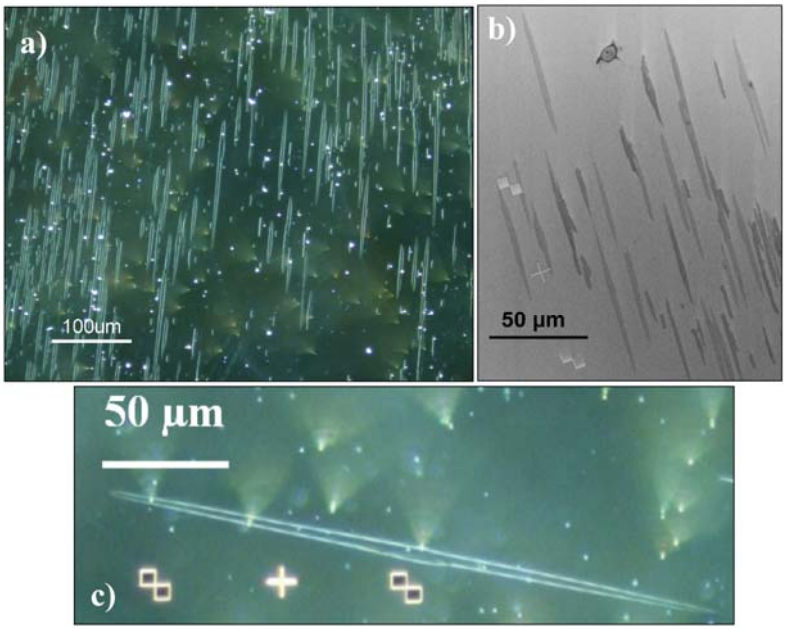

Figure 9: (a) Wide range Optical Microscopy in dark field view of samples annealed at 1700°C during 15min under SSV covered by a graphite cap. The C-face surface of this 6H-SiC on axis sample is covered by very long monolayers of graphene ribbons. (b) Typical SEM image of the same sample. (c) OM in dark field mode of a sample annealed at the same temperature but for 30 min leading to much longer graphene ribbons in average.

In figure 9(a) and figure 9(b), most ribbons are in the range of 100 µm long and 4 µm wide. However, increasing the process time one can easily increase the size without changing much the width.

This is shown in Figure 9(c). This new OM picture, again taken in the dark field mode, is now for a sample grown at 1700°C for 30 minutes. The length of ribbon approaches 300 µm and the width is not much affected. Dislocations still exist, which appear as yellow cones in figure 9(a) and figure 9(c). However, they are not as efficient nucleation centers as before. In many cases, a defect (dislocation) can be seen at the starting point (center) of a ribbon (like in the case of ribbon in figure 9(c)) but this is not mandatory. Many ribbons exist without any identified defect at the origin. Conversely, dislocations exist which are not nucleation centers. This is clear from figure 9(c) and comes because, below and close to the long graphene ribbons, the SiC surface reorganizes with long and uniform terraces. This is a standard effect of step-bunching, well-known in Si and SiC technologies, it comes from the small initial miscut of the wafer surface with respect to the nominal 6H-SiC one.

As a matter of fact the result of step bunching, as probed by AFM in figure 10, is very similar to the facet nucleation mechanism already reported for <111> silicon. In both cases, this is because a minimal (critical) width of terrace (W_c) is needed before the surface reconstruction can proceed. For details, see Ref.[30, 31]. Once a seed as been formed by a dislocation or any kind of nucleating center, the reconstruction expands rapidly while graphene grows on the reconstructed parts of terraces. This explains the anisotropic rate and unusual length of the ribbons. As long as the terrace width is lower than the critical value W_c, no surface reconstruction can be made. This stops the graphene growth perpendicular to the direction of terraces. As a result, the graphene layer expands preferentially on one isolated terrace and, at the end of the process, almost all the graphene ribbons occupy a single terrace surrounded by sharp and high edges. Time to time, the graphene layer expands on 2 or 3 terraces, probably depending on the size of the initial defect that initiates the growth.

Opposite to graphene exfoliated on a pre-oxidized Si wafer, epitaxial graphene grown on SiC is almost invisible by naked eye [32]. Using OM, what is actually seen in figure 9(a) and Figure 9(c) is not directly graphene layers but the underlying effect of surface reconstruction which increases the reflected light at the bunched edges. To really see the graphene ribbons one has to probe the sample by SEM as seen in figure 9(b) or, for more details, by AFM as seen in figure 10.

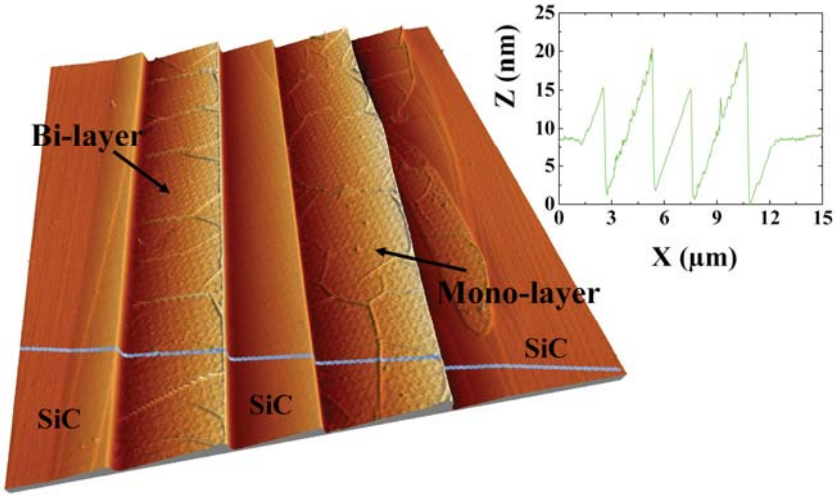

Figure 10: AFM picture of sample graphitized at 1700ºC during 15 min with a graphitic cap covering the sample. Two long graphene layers are seen on single large terraces. Above one of the terraces, a monolayer is laying while a Bernal bilayer AB is laying on the other one. The graphene layers are surrounded by step bunched bare SiC. The corresponding profile indicate that very high steps in the range of 10-20 nm high are detected while on this example the ribbons are 3-4 µm large.

From AFM one finds that the edges of graphene ribbons always coincide with the edges of terrace. They are atomically flat and exhibit wrinkles as already found on graphite material grown on SiC [33]. These wrinkles are few nanometers high and come because of the weak interaction between the first graphene ribbon and the underlying substrate. They give a first evidence that, on the C-face, the first graphene layer is almost free-standing, in strong opposition to the first layer of graphene grown on the Si-face of a SiC substrate. In this case the first graphene layer is strongly coupled to the buffer layer that the strain cannot relax and it does ***not*** exhibit wrinkles. On the C-face, the situation is just the opposite and the stress in the layer is almost completely relaxed. Results of optical investigations performed in the next section will confirm this (almost) free-standing character of EG ribbons grown on the C-face of on-axis SiC wafers.

6. Thickness and thickness uniformity

To probe the thickness and thickness uniformity of such EG ribbons, several tools can be used. They complemented each other and ascertained the results. Among them are differential micro-transmission

measurements, complemented by simultaneous collection of micro-Raman spectra. A schematic view of the experimental set-up is shown in figure 11.

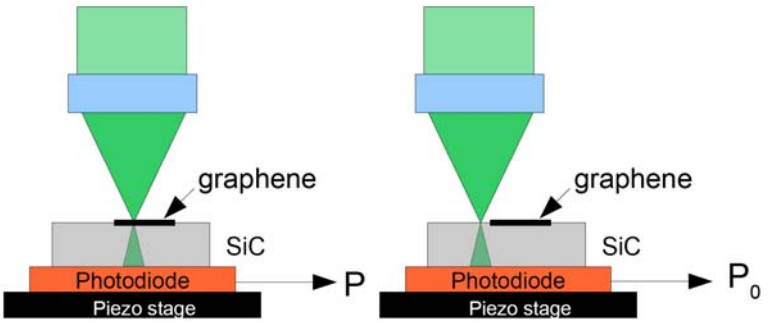

Figure. 11. Experimental set up used to perform combined μ-Raman and differential μ-transmission experiments.

Differential micro-transmission measurements. Experimental optical transmission measurements performed through suspended monolayer and bilayer graphene in air have confirmed the theoretical prediction that optical conductivity of the graphene monolayer is $\sigma = e^2/4\hbar$ [34]. The transmittance of a graphene layer on top of a substrate can be then calculated theoretically, and this has been done in the work of Stauber *et. al.* [35]. The point is to consider a single interface between two different media (usually air and substrate) with boundary conditions for the electromagnetic field modified by the presence of the graphene layer. On SiC, the electrical permittivity of the media is $\varepsilon_1 = 1.0$ for air and $\varepsilon_2 = 7.20$ for SiC, respectively. This gives for the transmittance of a monolayer graphene on a SiC substrate $T = 0.7814$ while, without any graphene on top (bare SiC substrate), the transmittance is $T_0 = 0.7912$. The relative extinction coefficient $\eta = (T_0\text{-}T)/T_0$ is then (theoretically) 1.23 % for a graphene monolayer on top of a SiC wafer. Since a bilayer has an optical conductivity twice as large as a monolayer in the visible range [36] it should result in a relative extinction coefficient of 2.44 %. Of course, the actual transmittance of the sample depends also on the backside (SiC/air interface). In this work it was optically polished but, if not but still homogeneous, this simply involves a common factor that cancels out, so that η depends only on the relative transmittance change through the first interface.

As an example let us consider the graphene ribbon shown in figure 12(a). To ascertain the thickness of this layer we performed 11 differential transmission measurements along the 11 different points. Using a piezo-motor to move the sample, we could plot η versus laser spot positions separated by 1 μm

distance. The experimental values obtained in this way for the extinction coefficient superimpose well to a broadened theoretical curve as shown in figure 12(b). To evaluate the noise related to the power measurements, successive acquisitions were done without changing position. In this way an average value $\eta = 1.18 \pm 0.06$ % (with coverage factor of 3) was found. Without any ambiguity, this confirms that the central part of the layer shown in Figure 12(a) is pure monolayer graphene.

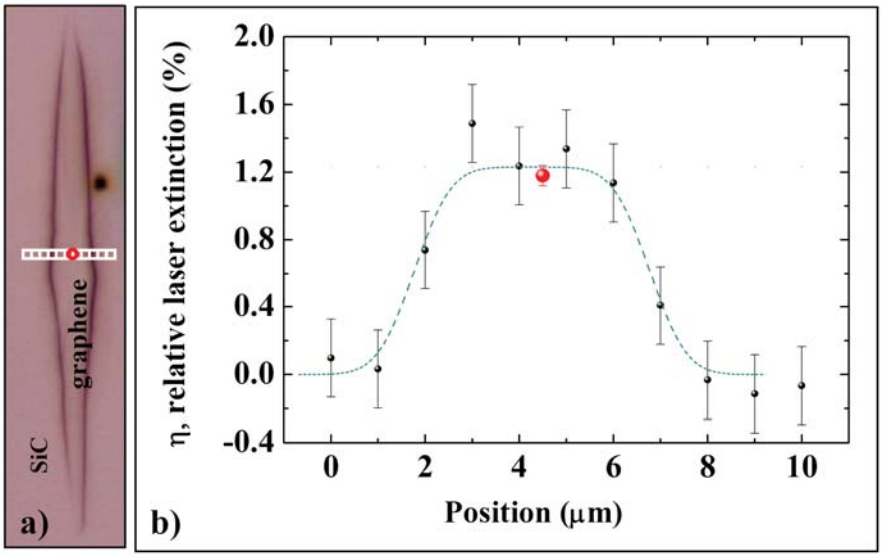

Figure 12: (a) OM view in the dark field mode of the graphene ribbon used to perform differential micro-transmission measurements; (b) Black point: linear scan of $\eta = (T_0\text{-}T)/T_0$ along the 10 μm white bar shown in (a); dash line: theoretical value computed for a graphene monolayer on SiC by convolution a 4μm wide ribbon with a Gaussian laser beam (FWHM = 1 μm).

Combining differential micro-transmission with micro-Raman spectroscopy. Of course, during differential micro-transmission measurements micro-Raman spectra can be systematically collected using the same excitation frequency (514 nm laser line of an Ar^+-ion laser). A typical result collected on the monolayer ribbon of figure 12(a) is shown in figure 13. Also shown, superimposed for convenience, a spectrum collected on a "classical" exfoliated monolayer graphene flake. Notice the strong similarity. The 2D-band shows a single peak (with a single lorentzian shape) centred at ~ 2685 ± 3 cm^{-1} while the full width at half maximum (FWHM) is about 25 cm^{-1}. The G-band falls between 1583 and 1587 cm^{-1}, with a FWHM of the order of 13 cm^{-1} which prove that the doping is rather low [37].

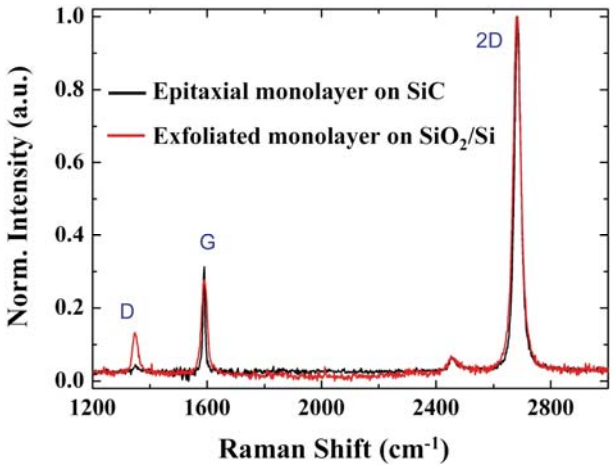

Figure 13: Typical Raman spectra collected on epitaxial graphene monolayer grown on the C-face of a SiC substrate heated at 1700ºC with a graphitic cap covering the surface, and on a monolayer graphene exfoliated on SiO_2 on Si.

While the ratio of integrated intensities I_{2D}/I_G for such monolayer graphene ranges from 5 to 8, the most striking result is that the 2D and G bands in EG ribbons are not significantly shifted to higher frequencies with respect to exfoliated graphene. This is a most important difference with respect to many previous works in which EG on the Si-face of a SiC wafer was considered. On such samples, a high level of residual thermal stress is constantly observed [18, 38, 39]. In this work, we observed that on the C-face, the stress was relaxed by the formation of wrinkles, as already shown in the AFM picture of figure 10. Such stress-relaxation mechanism has been observed on all samples investigated in this work and, altogether with the fact that we have almost no D-band, suggests the growth of high quality, lightly doped and basically strain relaxed almost free-standing graphene monolayers.

Mapping. Once we know that we are able to grow EG monolayer ribbons on the C-face of a 6H-SiC substrate (low doped and almost free-standing) the last experiment to be done is to validate the growth procedure by evaluating the homogeneity of layers. As an example, we display in figure 14 some of the Raman maps collected on the flakes already seen by AFM in figure 10. These 20 x 100 μm^2 maps were collected when probing with a step separation of 0.5 µm in X and 2 µm in Y the neighbouring ribbons seen in Figure 10.

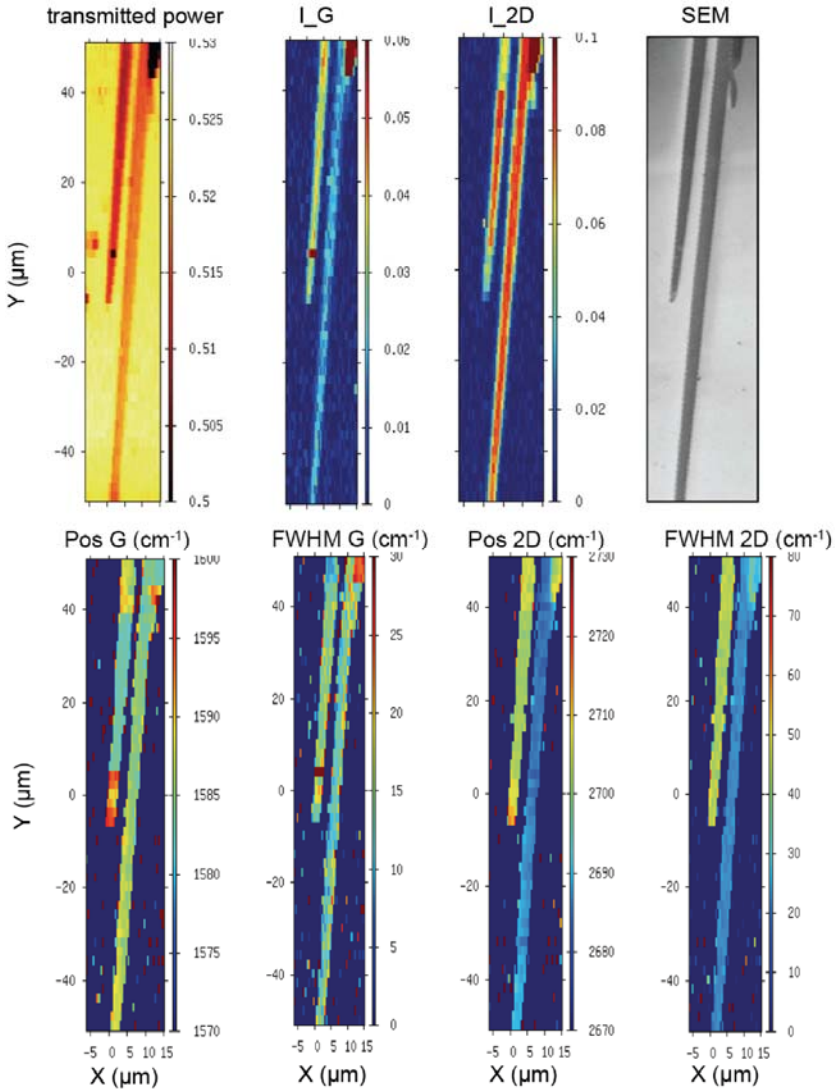

Figure 14. 20 µm x 100 µm maps collected on the two graphene ribbons shown in figure 10. They have been grown on the C-face of a 6H-SiC substrate covered with a graphite cap. The step size is 0.5 µm and 2 µm for the X and Y axis, respectively. The different maps refer to the power transmitted through the sample, the integrated intensities of the G and 2D Raman bands as well as the 2D-band and G-band frequencies and FWHM, respectively. The SEM image of the same (mapped) area is reported for comparison.

Because of the limited range of the XY piezo-displacement stage (100 × 100 μm^2) the two ribbons could not be completely probed simultaneously. However, already, the transmission map shows that they have excellent thickness uniformity. They show also that the left ribbon, which gives a weaker transmitted intensity, is thicker than the right one. To know the corresponding thicknesses, we start again from the transmitted power, complemented by additional point by point measurements. In this way we found that the right ribbon has a relative extinction η ranging from 1.2 to 1.4 %, confirming

without ambiguity that it is a true monolayer ribbon, while the second ribbon (on the left) has a relative extinction η ranging from 2.6 to 2.8 %, which corresponds to a bilayer ribbon.

All spectra collected on the same ribbon were almost identical. This confirms the potential of the method to grow large, uniform, monolayer graphene ribbons on the C-face of SiC wafers. However, concerning the bilayer ribbons, we found two different results. The first one, noticed AB in figure 15, comes from the left ribbon of figure 14. It is typical of Bernal stacking [23] but this result is not systematic. On some other ribbons (not shown) we found a completly different type of Raman spectra. The peak remains narrow but becomes two times more intense than the one collected on monolayer graphene, giving clear evidence of misoriented AA' stacking. For convenience, such a bilayer spectrum is shown as AA' in figure 15. It shows that, without measuring the transmitted power, it is hard to distinguish from simple Raman spectroscopy between a real monolayer with η =1.33% and two twisted bilayers with η =2.50%.

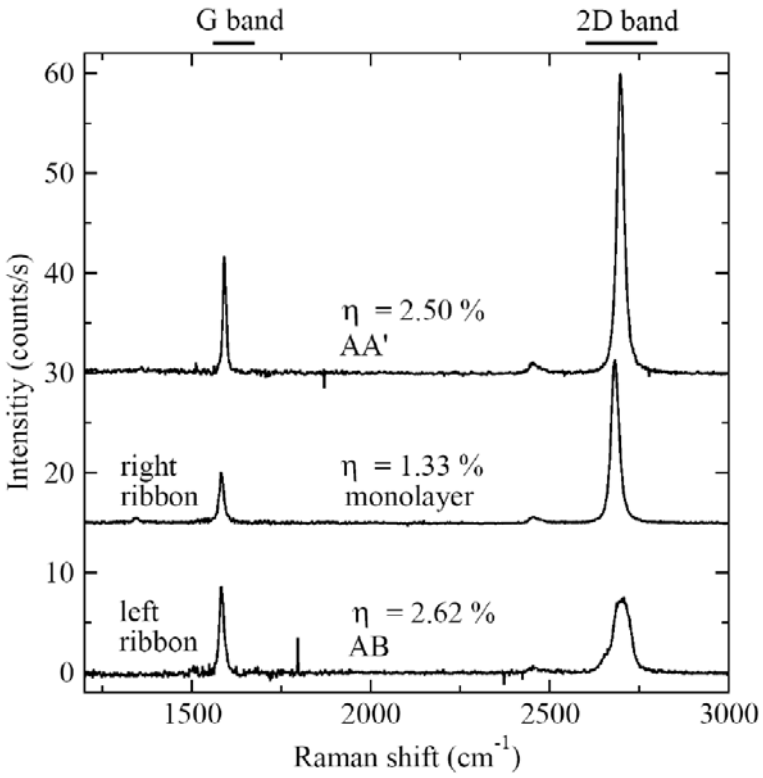

Figure. 15. Comparison of Raman spectra collected in the middle of different graphene ribbons. The relative extinction values ($\eta = \Delta T/T_0$) are also given. From top to bottom are identified: a misoriented bilayer (AA'), a monolayer, and a Bernal stacked bilayer (AB). The monolayer and AB bilayer come from the right and left ribbons visible in figure 14, respectively. The AA' bilayer comes from a different part.

7. Processing and collecting electrical results

Processing. On some monolayer ribbons, standard Hall bars have been defined using electron-beam lithography techniques. An example of such a device is shown in figure 16. The total length of the contacted monolayer is 25 µm, with a distance L = 10 µm between the lateral probes and a width W=1 µm between the Hall probes.

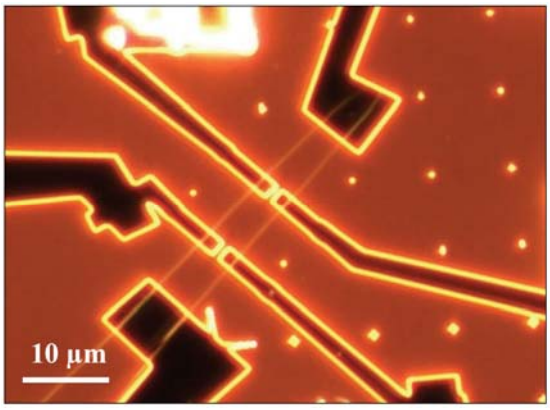

Figure. 16. Dark field image of a ribbon connected with 6 different contacts. The contacts define a Hall bar of 25 µm length and 5 µm width. The distance between two lateral probes is about 10 µm, the separation between 2 Hall probes across the ribbon is 1 µm.

Electrical results. Graphene layers grown on the Si-face of SiC substrates are well-known to be highly n-type doped. This comes from the charge transfer between the buffer layer and the first graphene layer. In the case of graphene grown on the C-face, we still observe a carrier concentration ranging from $5x10^{12}$ to $5x10^{13}$ cm^{-2} but, from the sign of the Hall effect, the carriers are holes. This high concentration of holes in the layer is probably not intrinsic. PMMA is known as p-type dopant, even for exfoliated graphene, and most probably the residual p-type doping comes because the attempts we made to clean the sample before electrical measurement were not successful enough. Of course, with such concentrations, the mobility is rather weak: about 2.000 cm^2/Vs at low temperature (~ 4K).

To date, increasing the mobility is only a matter of optimisation of the last cleaning sequence. Basically, one needs to heat up the sample to ~ 400ºC under H_2/Ar in order to burn all PMMA traces without destroying the device [40]. Fortunately, whatever are the hole density and mobility, Shubnikov-de Haas (SdH) oscillations could be recorded at low temperatures. Results are shown in Figure 17 when sweeping the perpendicular magnetic field from 0 to 13,5 T. Each maximum of the SdH oscillations

corresponds to the crossing of a Landau level with a given index with the Fermi energy. The Landau plot corresponds to the 1/B position of the SdH maxima as a function of the Landau level index. It is shown in the inset of Figure 17. Notice that the maxima align along a line which crosses the origin, this is the usual signature of graphene monolayers and uncoupled graphene layers [41].

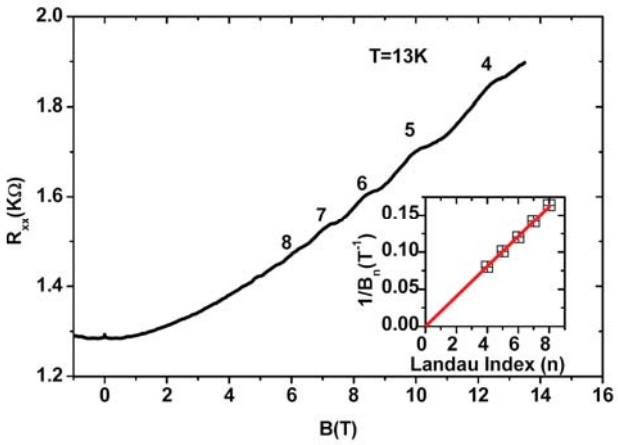

Figure. 17. Magnetoresistance of the device shown in figure 16. At 13K we find clear SdH oscillations. The Landau level indexes are reported over each resistance maximum. Insert: Landau plot (position of the resistance maxima as a function of their index). The maxima are aligned along a straight line which crosses the origin.

To strengthen this conclusion, we have used the temperature dependence of the SdH oscillations to extract the cyclotron mass (m_c). We know that the amplitude of oscillations is proportional to $\gamma/\sinh(\gamma)$ in which $\gamma = 2\pi^2 k_B T m_c/eB$ [42]. However, the magnetoresistance shows superimposed to the SdH oscillations a weak power-law dependent magnetoresistivity ($\sim B^{1.33}$). Such a power law is common in HOPG graphite and, among the possible explanations, the simplest one is that the current path changes with B due to sample inhomogeneity [43]. In our case, the origin of inhomogeneities may be wrinkles or residual traces of the PMMA film. In figure 18(a) we show the oscillatory part of the magnetoresistance $\Delta R_{xx}(B,T)$ after subtracting this power law dependence.

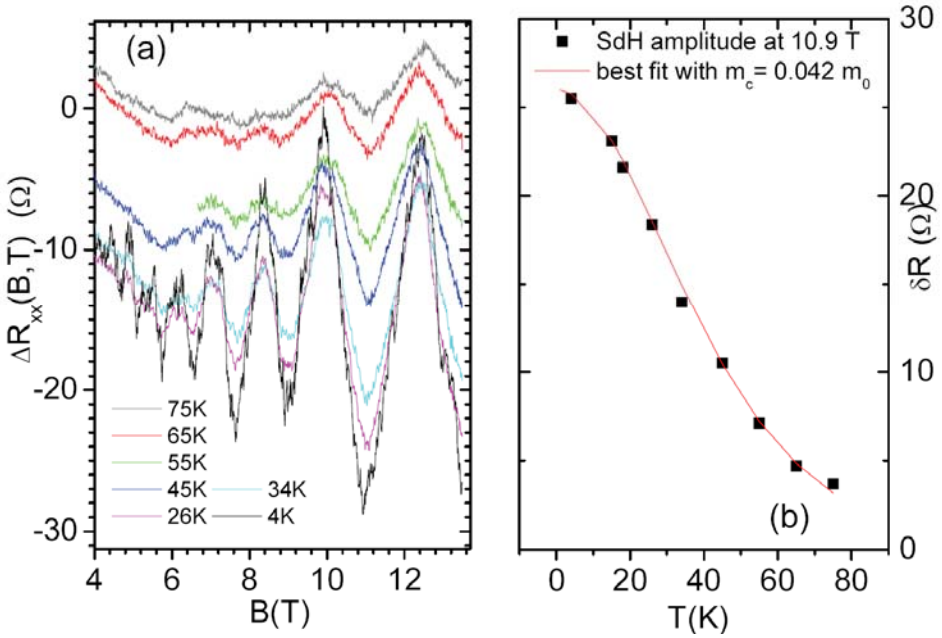

Figure. 18. (a) Longitudinal resistance at various temperatures (from 4K to 80K). The damping of the oscillations with T allows for the extraction of the cyclotron mass. (b) Best fit gives a cyclotron mass of 0.042 m_0, and a corresponding carrier density $5x10^{12}$ cm^{-2}. The latter value is in agreement with the carrier density extracted from the SdH frequency.

The SdH amplitude decreases when T increases but, still, has not disappeared at T=80K. The amplitude δR of the main oscillation at B=10.6 T is plotted in figure 18(b), with the best fit giving a cyclotron mass $m_c = 0.042m_0$. For a graphene film this mass corresponds to a carrier density $n_s = m_c^2v^2/\pi\hbar^2 \sim 5x10^{12}$ cm^{-2}. This concentration is in good agreement with the frequency of SdH oscillations $f \sim 100.0$ $T^{-1} = \pi\hbar n_s/2e$. It corresponds also to the Hall concentration given by Hall measurements.

8. Conclusion

Reviewing the growth of self-ordered epitaxial graphene ribbons on the C-face of 6H-SiC substrates, we have shown that this necessitates to work at high temperature (~1700°C) and to use a graphite cap to lower the sublimation of Si species. Then, long homogeneous graphene ribbons start to grow spontaneously on the C-face of the SiC substrates. These ribbons are all oriented in the same direction, with wrinkles-free areas of several μm^2, and fully occupy a single terrace of the reconstructed, step-bunched, SiC surface. They can be several hundred of μm long depending on the temperature and time of the process. Raman spectroscopy indicates high quality, slightly strained, homogeneous ribbons. A

standard Raman spectrum of graphene monolayer epitaxied on the C-face of a SiC wafer is presented for the first time and is expected to become a reference. In addition, we have shown that optical differential transmission is an easy and successfully tool to prove the monolayer character of ribbons. When working on transparent substrates like SiC, we expect this technique to spread widely as a companion tool for Raman. This is indeed a very simple and reliable technique that consists in measuring, with a high sensitivity power meter, the laser power transmitted through the sample during the acquisition of micro-Raman spectra. This is only possible because SiC is transparent to the usual laser wavelength, contrary to oxidized silicon substrates. Finally, the last test that has to be past to guaranty the quality and homogeneity of the epitaxied graphene layers is the fabrication of a device and its electrical characterization. The Hall Bars devices investigated in this work are p-type doped with a phase of SdH oscillations typical for graphene layers.

ACKNOWLEDGMENTS: We greatly acknowledge Jean-Roch Huntzinger from GES (Montpellier) and Laurence Magaud from Institut Néel (Grenoble) for fruitful comment and discussion. We also acknowledge the EC for partial support through the RTN "ManSiC" Project (Grant MRTN-CT-2006-035735). The French ANR is also acknowledged for supporting the work through the Project Blanc 2006 "GraphSiC". Finally, one of us (N.C.) acknowledges the Spanish Government for a Grant "Juan de la Cierva 2006".

REFERENCES:

[1] Novoselov K S, Geim A K, Morozov S V, Jiang D, Zhang Y, Dubonos S V, Grigorieva I V and Firsov A A 2004 *Science* **306** 666-9

[2] Berger C, Song Z M, Li T B, Li X B, Ogbazghi A Y, Feng R, Dai Z T, Marchenkov A N, Conrad E H, First P N and de Heer W A 2004 *J. Phys. Chem. B* **108** 19912

[3] Novoselov K S, Geim A K, Morozov S V, Jiang D, Katsnelson M I, Grigorieva I V, Dubonos S V and Firsov A A 2005 *Nature* **438** 197

[4] http://www.itrs.net In: *ITRS: Emerging Research materials 2009,*

[5] Hernandez Y, Nicolosi V, Lotya M, Blighe F M, Sun Z, De S, McGovern I T, Holland B, Byrne M, Gun'Ko Y K, Boland J J, Niraj P, Duesberg G, Krishnamurthy S, Goodhue R, Hutchison J, Scardaci V, Ferrari A C and Coleman J N 2008 *Nature Nanotechnology* **3** 563

[6] Sutter P 2009 *Nature Materials* **8** 171-2

[7] Li X S, Cai W W, An J H, Kim S, Nah J, Yang D X, Piner R, Velamakanni A, Jung I, Tutuc E, Banerjee S K, Colombo L and Ruoff R S 2009 *Science* **324** 1312-4

[8] Dato A, Radmilovic V, Lee Z H, Phillips J and Frenklach M 2008 *Nano Lett.* **8** 2012

[9] Berger C, Song Z M, Li X B, Wu X S, Brown N, Naud C, Mayo D, Li T B, Hass J, Marchenkov A N, Conrad E H, First P N and de Heer W A 2006 *Science* **312** 1191-6

[10] Tzalenchuk A, Lara-Avila S, Kalaboukhov A, Paolillo S, Syväjarvi M, Yakimova R, Kazakova O, Janssen T J B M, Fal'ko V I and Kubatkin S 2010 *Nat Nanotechnol* **5** 186

[11] Kedzierski J, Hsu P L, Healey P, Wyatt P W, Keast C L, Sprinkle M, Berger C and de Heer W A 2008 *IEEE Transactions on Electron Devices* **55** 2078

[12] Lin Y M, Dimitrakopoulos C, Jenkins K A, Farmer D B, Chiu H Y, Grill A and Avouris P 2010 *Science* **327** 662

[13] Hass J, Feng R, Li T, Li X, Zong Z, de Heer W A, First P N, Conrad E H, Jeffrey C A and Berger C 2006 *Applied Physics Letters* **89** 143106

[14] Hass J, Feng R, Millan-Otoya J E, Li X, Sprinkle M, First P N, de Heer W A, Conrad E H and Berger C 2007 *Physical Review B* **75** 214109

[15] de Heer W A, Berger C, Wu X S, First P N, Conrad E H, Li X B, Li T B, Sprinkle M, Hass J, Sadowski M L, Potemski M and Martinez G 2007 *Solid State Communications* **143** 92

[16] Virojanadara C, Syvajarvi M, Yakimova R, Johansson L I, Zakharov A A and Balasubramanian T 2008 *Physical Review B* **78** 245403

[17] Emtsev K V, Bostwick A, Horn K, Jobst J, Kellogg G L, Ley L, McChesney J L, Ohta T, Reshanov S A, Rohrl J, Rotenberg E, Schmid A K, Waldmann D, Weber H B and Seyller T 2009 *Nature Materials* **8** 203-7

[18] Lee D S, Riedl C, Krauss B, von Klitzing K, Starke U and Smet J H 2008 *Nano Lett.* **8** 4320-5

[19] http://www.novasic.com/

[20] http://www.annealsys.com/

[21] Camara N, Rius G, Huntzinger J-R, Tiberj A, Magaud L, Mestres N, Godignon P and Camassel J 2008 *Applied Physics Letters* **93** 263102

[22] Biedermann L B, Bolen M L, Capano M A, Zemlyanov D and Reifenberger R G 2009 *Physical Review B* **79** 125411

[23] Ferrari A C, Meyer J C, Scardaci V, Casiraghi C, Lazzeri M, Mauri F, Piscanec S, Jiang D, Novoselov K S, Roth S and Geim A K 2006 *Physical Review Letters* **97** 187401

[24] Faugeras C, Nerriere A, Potemski M, Mahmood A, Dujardin E, Berger C and de Heer W A 2008 *Applied Physics Letters* **92** 011914

[25] Rohrl J, Hundhausen M, Emtsev K V, Th S, Graupner R and Ley L 2008 *Applied Physics Letters* **92** 201918

[26] Stone A J and Wales D J 1986 *Chem. Phys. Lett.* **128** 501

[27] Hass J, de Heer W A and Conrad E H 2008 *J. Phys.: Condens. Matter* **20** 323202

[28] Poncharal P, Ayari A, Michel T and Sauvajol J L 2008 *Physical Review B* **78** 113407

[29] Hass J, Varchon F, Millan-Otoya J E, Sprinkle M, Sharma N, De Heer W A, Berger C, First P N, Magaud L and Conrad E H 2008 *Physical Review Letters* **100** 125504

[30] Camara N, Huntzinger J R, Rius G, Tiberj A, Mestres N, Perez-Murano F, Godignon P and Camassel J 2009 *Physical Review B* **80** 125410

[31] Jeong H C and Weeks J D 1998 *Physical Review B* **57** 3939-48

[32] Abergel D S L, Russell A and Fal'ko V I 2007 *Applied Physics Letters* **91** 063125

[33] Cambaz Z G, Yushin G, Osswald S, Mochalin V and Goyotsi Y 2008 *Carbon* **46** 841-9

[34] Nair R R, Blake P, Grigorenko A N, Novoselov K S, Booth T J, Stauber T, Peres N M R and Geim A K 2008 *Science* **320** 1308

[35] Stauber T, Peres N M R and Geim A K 2008 *Physical Review B* **78** 085432

[36] Abergel D S L and Fal'ko V I 2007 *Physical Review B* **75** 155430

[37] Das A, Pisana S, Chakraborty B, Piscanec S, Saha S K, Waghmare U V, Novoselov K S, Krishnamurthy H R, Geim A K, Ferrari A C and Sood A K 2008 *Nature Nanotechnology* **3** 210

[38] Ni Z H, Chen W, Fan X F, Kuo J L, Yu T, Wee A T S and Shen Z X 2008 *Physical Review B* **77** 115416

[39] Ferralis N, Maboudian R and Carraro C 2008 *Physical Review Letters* **101** 156801

[40] Ishigami M, Chen J H, Cullen W G, Fuhrer M S and Williams E D 2007 *Nano Lett.* **7** 1643-8

[41] Berger C, Wu X, First P N, Conrad E H, Li X, Sprinkle M, Hass J, Varchon F, Magaud L, Sadowski M L, Potemski M, Martinez G and De Heer W A 2008 *Advances in Solid State Physics* **47** 145

[42] Gusynin V P and Sharapov S G 2005 *Phys. Rev. B* **71** 125124

[43] Parish M and Littlewood P B 2003 *Nature* **426** 162